Cell

# Conserved MicroRNA miR-8/miR-200 and Its Target USH/FOG2 Control Growth by Regulating PI3K

Seogang Hyun,[1,3] Jung Hyun Lee,[1,3] Hua Jin,[1,3] JinWu Nam,[1] Bumjin Namkoong,[1] Gina Lee,[2] Jongkyeong Chung,[2] and V. Narry Kim[1,*]
[1]School of Biological Sciences and National Creative Research Center, Seoul National University, Seoul, 151-742, Korea
[2]Department of Biological Sciences and National Creative Research Center, Korea Advanced Institute of Science and Technology, Daejon, 305-701, Korea
[3]These authors contributed equally to this work
*Correspondence: narrykim@snu.ac.kr
DOI 10.1016/j.cell.2009.11.020

## SUMMARY

How body size is determined is a long-standing question in biology, yet its regulatory mechanisms remain largely unknown. Here, we find that a conserved microRNA miR-8 and its target, USH, regulate body size in *Drosophila.* miR-8 null flies are smaller in size and defective in insulin signaling in fat body that is the fly counterpart of liver and adipose tissue. Fat body-specific expression and clonal analyses reveal that miR-8 activates PI3K, thereby promoting fat cell growth cell-autonomously and enhancing organismal growth non-cell-autonomously. Comparative analyses identify USH and its human homolog, FOG2, as the targets of fly miR-8 and human miR-200, respectively. USH/FOG2 inhibits PI3K activity, suppressing cell growth in both flies and humans. FOG2 directly binds to p85α, the regulatory subunit of PI3K, and interferes with the formation of a PI3K complex. Our study identifies two novel regulators of insulin signaling, miR-8/miR-200 and USH/FOG2, and suggests their roles in adolescent growth, aging, and cancer.

## INTRODUCTION

Animal body size is a biological parameter subject to considerable stabilizing selection; animals of abnormal size are strongly selected against as less fit for survival. Thus, the way in which body size is determined and regulated is a fundamental biological question. Recent studies using insect model systems have begun to provide some clues by showing that insulin signaling plays an important part in modulating body growth (Ikeya et al., 2002; Rulifson et al., 2002). The binding of insulin (insulin-like peptides in *Drosophila*) to its receptor (InR) triggers a phosphorylation cascade involving the insulin receptor substrate (IRS; chico in *Drosophila*), phosphoinositide-3 kinase (PI3K), and Akt/PKB (Edgar, 2006). An active PI3K complex consists of a catalytic subunit (p110; dp110 in *Drosophila*) and a regulatory subunit (p85α; dp60 in *Drosophila*). Phosphorylated Akt (p-Akt) phosphorylates many proteins—including forkhead box O transcription factor (FOXO) —which are involved in cell death, cell proliferation, metabolism, and life span control (Arden, 2008). Once activated, the kinase cascade enhances cell growth and proliferation.

Organismal growth is achieved not only by cell-autonomous regulation but also by non-cell-autonomous control through circulating growth hormones (Baker et al., 1993; Edgar, 2006). Recent studies in insects indicate that several endocrine organs, such as the prothoracic gland and fat body, govern organismal growth by coordinating developmental and nutritional conditions (Caldwell et al., 2005; Colombani et al., 2005; Colombani et al., 2003; Mirth et al., 2005). However, detailed mechanisms of how body size is determined and modulated remain largely unknown.

microRNAs (miRNAs) are noncoding RNAs of ~22 nt that act as posttranscriptional repressors by base-pairing to the 3′ untranslated region (UTR) of their cognate mRNAs (Bartel, 2009). The physiological functions of individual miRNAs remain largely unknown. Studies of miRNA function rely heavily on computational algorithms that predict target genes (John et al., 2004; Kim et al., 2006; Kiriakidou et al., 2004; Krek et al., 2005; Lewis et al., 2005; Stark et al., 2003). In spite of their utility, however, these target prediction programs generate many false-positive results, because regulation in vivo depends on target message availability and complementary sequence accessibility. To overcome the difficulties in identifying real targets, various experimental approaches have been developed, including microarrays, proteomic analyses, and biochemical purification of the miRNA-mRNA complex (Bartel, 2009). Genetic approaches using model organisms can also be useful tools for studying the biological roles of miRNAs at both the organismal and molecular levels (Smibert and Lai, 2008). Despite these advances, however, it is still a daunting task to understand the biological function of a given miRNA and to identify its physiologically relevant targets.

Here, we find using *Drosophila* as a model system that conserved miRNA miR-8 positively regulates body size by

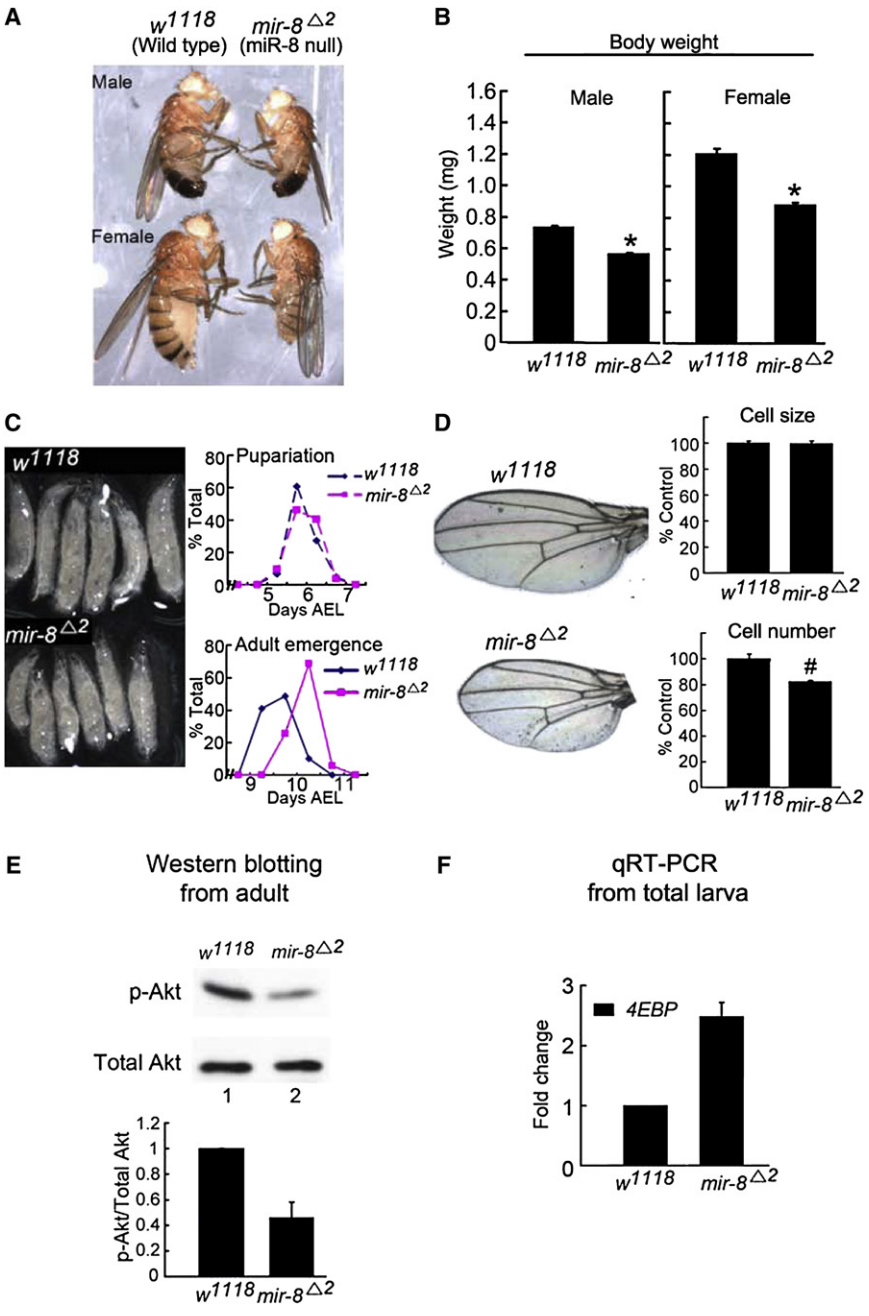


**Figure 1. Growth Defect of *mir-8* Mutant**

(A) Both male and female miR-8 null flies are smaller than their wild-type counterparts.

(B) Average weight of wild-type (male, $n$ = 65; female, $n$ = 70) and miR-8 null (male, $n$ = 60; female, $n$ = 40) flies.

(C) Left: miR-8 null larvae show retarded growth phenotype. The larval photograph was taken 100 hr AEL (after egg laying). Right: miR-8 null larvae pupariate at normal time points ($w^{1118}$, $n$ = 290; $mir\text{-}8^{\Delta 2}$, $n$ = 104) and are slightly delayed in adult emergence ($w^{1118}$, $n$ = 248; $mir\text{-}8^{\Delta 2}$, $n$ = 70).

(D) Left: miR-8 null flies have reduced wing size. Right: miR-8 null flies have reduced wing cell number with no significant change in cell size ($w^{1118}$, $n$ = 10; $mir\text{-}8^{\Delta 2}$, $n$ = 8).

(E) Reduced level of phospho-Akt (p-Akt) in miR-8 null flies. Measurements were made in triplicate.

(F) Increased level of a FOXO target gene (4EBP) in miR-8 null larvae as determined by qRT-PCR. $^{*}p < 2.9 \times 10^{-10}$; $^{\#}p < 3.9 \times 10^{-4}$, compared with wild-type. Error bars denote the standard error of the mean (SEM).

targeting a fly gene called *u-shaped* (*ush*) in fat body cells. We further discover that this function of miR-8 and USH is conserved in mammals and that the human homolog of USH, FOG2, acts by directly binding to the regulatory subunit of PI3K.

## RESULTS

### Small Body Phenotype of the *mir-8* Mutant

In a screen for miRNAs that modulate cell proliferation, we observed that human miR-200 miRNAs (miR-200a, miR-200b, miR-200c, miR-141, and miR-429) promote cell growth when transfected into several human cell lines (Park et al., 2009) (see Figure S1 available online). Members of the miR-200 family are upregulated in certain cancers, including ovarian cancer, consistent with our observation of the proliferation promoting effects (Iorio et al., 2007; Nam et al., 2008). Because the miR-200 family is highly conserved in bilaterian animals, with miR-8 being the sole homolog in *Drosophila melanogaster*, we used *D. melanogaster* in order to uncover the biological function of the miR-200 family.

We first analyzed the phenotype of the miR-8 null fly, $mir\text{-}8^{\Delta 2}$ (a generous gift from Steve Cohen) (Karres et al., 2007). It was previously shown that *mir-8* mutation results in increased apoptosis in the brain and frequent occurrence of malformed legs and wings (in about one-third of the mutants) (Karres et al., 2007). Interestingly, in addition to these phenotypes, we found that miR-8 null flies are significantly smaller in size (Figure 1A) and mass (Figure 1B) than their wild-type counterparts.

The determination of the final body size in insects during the larval stage is analogous to that which occurs during the human juvenile period (Edgar, 2006; Mirth and Riddiford, 2007). It is generally known that reduced body size in insects is caused by either slow larval growth, precocious early pupariation that shortens the larval growth period, or both (Colombani et al., 2003; Edgar, 2006; Mirth and Riddiford, 2007). We observed that, at 100 hr after egg laying (AEL), miR-8 null larvae exhibit a significantly smaller body volume than do wild-type larvae (Figure 1C, left). The onset of pupariation in miR-8 null flies was

not significantly different from that in wild-type flies (Figure 1C, upper right), and adult emergence was slightly delayed (~12 hr) (Figure 1C, lower right). Thus, the smaller body size of miR-8 null flies is likely to be caused by slower growth during the larval period rather than by precocious pupariation. Insufficient food intake has been reported to accompany either precocious or delayed pupariation, depending on the onset of reduced feeding (Layalle et al., 2008; Mirth et al., 2005). However, the levels of *Drosophila* insulin-like peptides (*Dilps*), which are known to be reduced in starvation conditions (Colombani et al., 2003; Ikeya et al., 2002), were not downregulated in miR-8 null larvae (data not shown). Given the unaffected onset time of pupariation (Figure 1C) and the levels of *Dilps* in this animal, the small body size of miR-8 null flies is unlikely due to reduced feeding.

Next, we asked whether the small body phenotype was caused by a reduction in cell size, cell number, or both. We measured wing cell size and number and found that cell number was reduced in the wing in miR-8 null flies, whereas cell size was not significantly different from that of wild-type (Figure 1D). Thus, assuming that similar regulation takes place in other body parts, the reduced growth in the peripheral tissues of the miR-8 null flies may be ascribed to decreased cell number rather than reduced cell size.

To understand why miR-8 null animals grow slowly, we examined the activities of the proteins involved in insulin signaling in the miR-8 null flies. We first determined the level of activated Akt by Western blotting using a p-Akt-specific antibody (Figure 1E). The p-Akt level was reduced in the mutant flies, suggesting that Akt signaling is impaired in the absence of miR-8 (Figure 1E). Activated p-Akt is known to inactivate FOXO via phosphorylation. Phosphorylation prevents nuclear localization of FOXO, which, in turn, results in the reduction of transcription of FOXO target genes. Consistent with the reduced level of p-Akt, the FOXO target gene, 4EBP, was increased in mir-8 mutant larvae (Figure 1F), indicating that insulin signaling is indeed significantly reduced in the miR-8 null animal.

## Fat Body-Specific Expression of miR-8 Rescues the Small Body Phenotype

We examined the spatial expression pattern of miR-8 in larvae using a *mir-8* enhancer trap GAL4 line (hereafter referred to as mir-8 gal4), which, when combined with *UAS-GFP*, expresses GFP under the control of the *mir-8* enhancer (Karres et al., 2007). In addition to the signals in the brain, wing discs, and leg discs that were previously observed by Cohen and colleagues (Karres et al., 2007), we noticed strong signals in the fat body (Figure 2A and data not shown). We also determined the level of miR-8 by Northern blotting using total RNA prepared from different larval organs, which showed that miR-8 is indeed highly abundant in the fat body (Figure 2B).

Recent studies suggested that *Drosophila* fat body may be an important organ in the control of energy metabolism and growth (Colombani et al., 2003, 2005; Edgar, 2006; Leopold and Perrimon, 2007). Therefore, we reasoned that if miR-8 in the larval fat body is critical for body size control, exclusive expression of miR-8 in the fat body alone should alleviate the whole body size defect observed in the mir-8 mutants. To test this idea, we generated transgenic flies to specifically reintroduce miR-8 into the fat bodies of mir-8 mutant larvae using a fat body–specific GAL4 driver, *Cg gal4* (*CgG4*) (Takata et al., 2004). Remarkably, miR-8 expression in the fat body alone rescued the phenotype to near wild-type levels in both body weight (Figure 2C, left) and body size (data not shown), suggesting that miR-8 in the fat body is important for systemic body growth. Another interesting observation was that the miRNAs from the human miR-200c cluster, which includes miR-200c and miR-141, could also yield a comparable rescue effect (Figure 2C). Human miR-200 family miRNAs, which are located in two chromosomal clusters, have extensive homology to miR-8 (Figure 3A). The fact that miRNAs of the human miR-200c cluster effectively compensate for the loss of miR-8 suggests that these human miRNAs can be processed by the *Drosophila* miRNA processing machinery and that they share a conserved biological function. Because *CgG4* is expressed in the anterior lymph gland as well as in the fat body (Asha et al., 2003), we used an additional GAL4 driver, *ppl gal4* (*pplG4*), that is active mainly in the fat body and slightly in the salivary gland (Zinke et al., 1999). Similar rescue effects were observed with *pplG4*, in support of the fat body–specific function of miR-8 (Figure 2C, right).

As mentioned above, miR-8 is also expressed in the central nervous system and prevents neurodegeneration (Karres et al., 2007). To examine whether miR-8 in neuronal cells participates in the regulation of organismal growth possibly by regulating feeding behavior indirectly, miR-8 was specifically expressed in neuronal cells by using *elav gal4* (*elavG4*) in miR-8 null animals. This genetic manipulation did not alleviate the dwarf phenotype of miR-8 null flies, indicating that the function of miR-8 in the fat body is spatiotemporally distinct from that in neuronal tissues (Figure 2D).

## USH Is a Critical Target of miR-8 in the Regulation of Body Growth

To further understand the molecular function of miR-8, we set out to identify miR-8 target genes responsible for body size control. Because miR-8 is a highly conserved miRNA and because the human homologs promote cell proliferation in human cells (Figure S1), we assumed that the targets involved in the cell proliferation phenotype may be conserved throughout evolution. To discover such conserved targets, we first listed the candidate target genes of both fly miR-8 and human miR-200 miRNAs using five different target prediction programs (Figure 3B): miRanda (John et al., 2004), miTarget (Kim et al., 2006), microT (Kiriakidou et al., 2004), PicTar (Krek et al., 2005), and TargetScan (Lewis et al., 2005). The two groups of putative targets, one from flies and the other from humans, were then compared with each other to identify homologous gene pairs. The *Drosophila* gene *u-shaped* (*ush*) and its human homolog *Friend of GATA 2* (*FOG2*, also known as *ZFPM2*) were the most frequently predicted gene pair conserved in both species. From the target candidate list, we selected 15 genes, including *ush*/*FOG2*, that are known as tumor suppressors or negative regulators of cell proliferation in at least one species (Table S1). We validated these target genes with luciferase reporter plasmids. Briefly, we inserted each target's 3′ UTR, which contains the miRNA target sites, downstream of a luciferase gene. The reporter activities were measured following

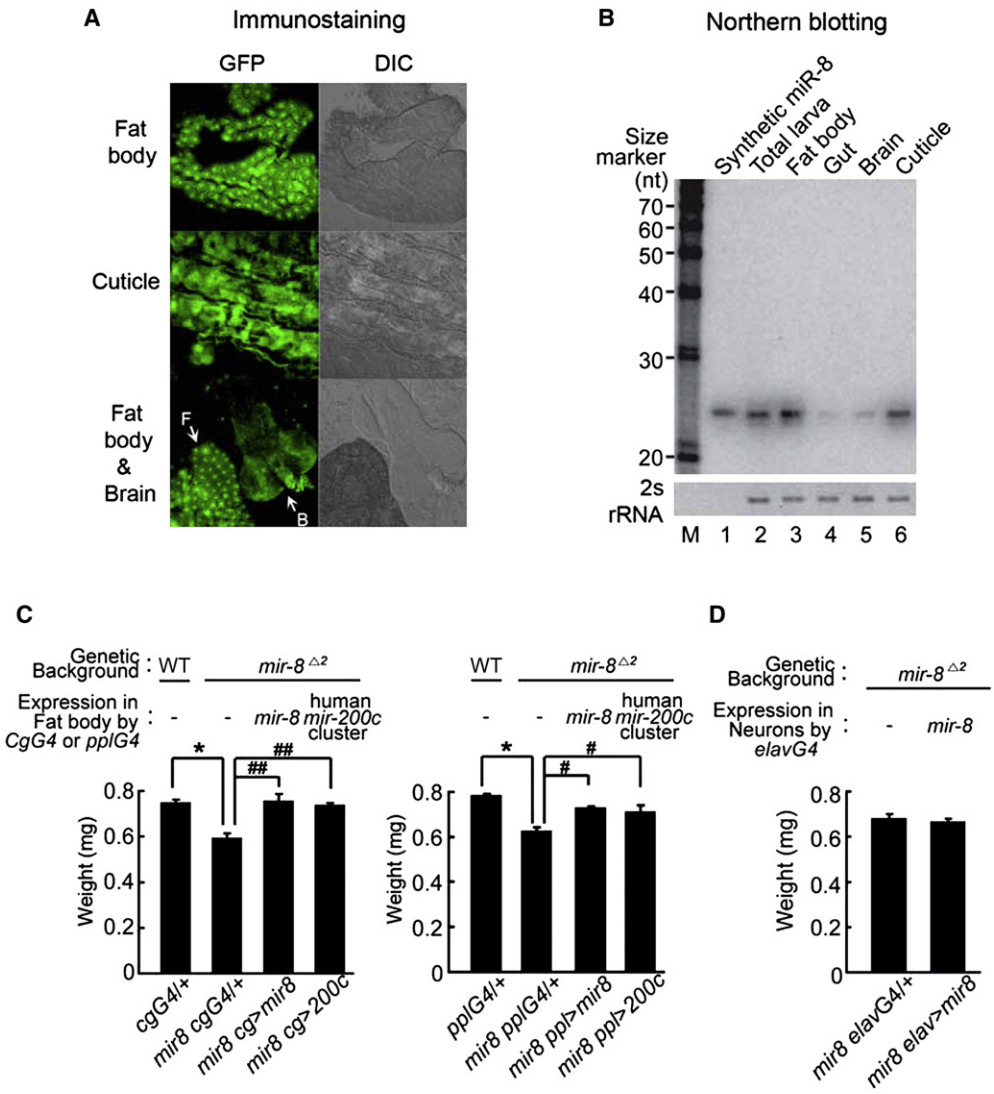


**Figure 2. miR-8 in Fat Body Regulates Body Growth**

(A) Expression of miR-8 in the larval fat body (denoted by "F"), brain (denoted by "B"), and cuticle is visualized using mir-8 *gal4*/*UAS-GFP*.

(B) miR-8 is highly expressed in the larval fat body. Larval organs were separated and analyzed by Northern blot. Synthetic miR-8 RNA (2 fmole) was included as a control.

(C) Expression of miR-8 or human miR-200c cluster in the fat body of miR-8 null larvae rescues the small body phenotype. Two fat body–specific GAL4 drivers (*Cg gal4* and *ppl gal4*) were used (left and right histograms, respectively). $n > 45$ male flies were used for each genotype. $^{*}p < 3 \times 10^{-10}$, compared with GAL4-only control. $^{\#\#}p < 1 \times 10^{-6}$; $^{\#}p < 0.0043$, compared with miR-8 null mutant having only the GAL4 transgene.

(D) Expression of miR-8 in neuronal cells did not rescue the small body phenotype of the miR-8 null animal. A neuronal specific GAL4 driver (*elav gal4*) was used, and $n > 30$ male flies were measured for each genotype.

cotransfection of miRNAs and the reporter plasmids into *Drosophila* S2 or human HeLa cells. After extensive reporter assays, we identified seven gene pairs that respond both to miR-8 and to miR-200 family miRNAs in fly and human cells, respectively (Figure 3C). The full data set is provided in Table S1.

To examine which targets among the candidates are physiologically relevant to the phenotype observed, we knocked down the candidate genes in the fat body of miR-8 null flies and asked whether the knockdown could rescue the small body phenotype. Using the UAS-RNA interference (RNAi) lines obtained from the Vienna RNAi Library Centre, dsRNAs of five candidate genes were expressed in the fat body of mir-8 mutants using *CgG4*. *Lap1* knockdown was unsuccessful and, thus, did not rescue the *mir-8* mutant phenotype (Figure S2 and data not shown). Among the RNAi lines tested, the one against *ush* rescued the dwarf phenotype most dramatically (Figure 3D, upper). RNAi of *ush* in wild-type background did not significantly increase body weight, ruling out the possibility that the effects of *ush* knockdown and *mir-8* mutation are additive (Figure 3D, lower).

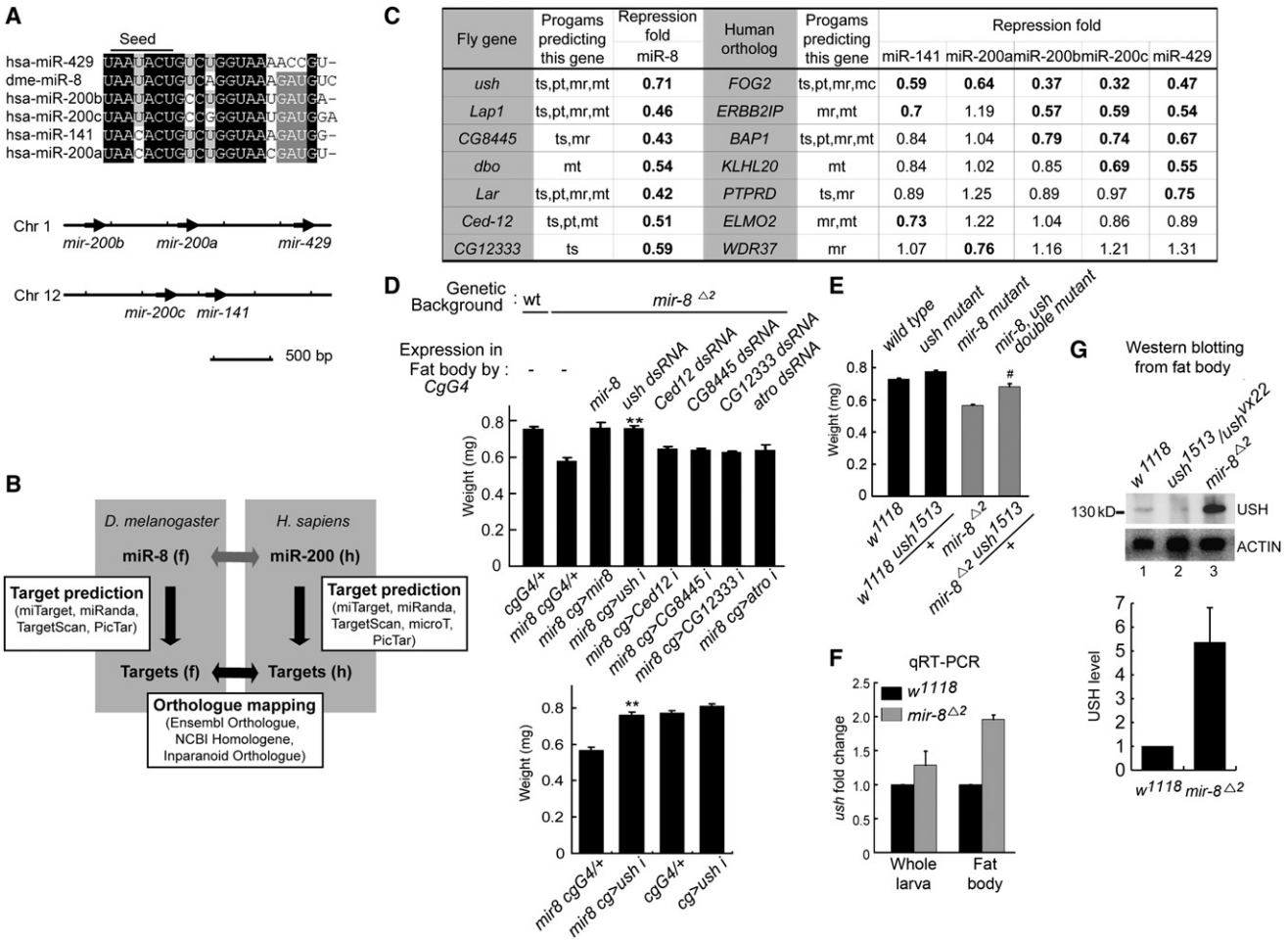


| Fly gene | Progams predicting this gene | Repression fold miR-8 | Human ortholog | Progams predicting this gene | Repression fold miR-141 | miR-200a | miR-200b | miR-200c | miR-429 |
|---|---|---|---|---|---|---|---|---|---|
| *ush* | ts,pt,mr,mt | **0.71** | *FOG2* | ts,pt,mr,mc | **0.59** | **0.64** | **0.37** | **0.32** | **0.47** |
| *Lap1* | ts,pt,mr,mt | **0.46** | *ERBB2IP* | mr,mt | **0.7** | 1.19 | **0.57** | **0.59** | **0.54** |
| *CG8445* | ts,mr | **0.43** | *BAP1* | ts,pt,mr,mt | 0.84 | 1.04 | **0.79** | **0.74** | **0.67** |
| *dbo* | mt | **0.54** | *KLHL20* | mt | 0.84 | 1.02 | 0.85 | **0.69** | **0.55** |
| *Lar* | ts,pt,mr,mt | **0.42** | *PTPRD* | ts,mr | 0.89 | 1.25 | 0.89 | 0.97 | **0.75** |
| *Ced-12* | ts,pt,mt | **0.51** | *ELMO2* | mr,mt | **0.73** | 1.22 | 1.04 | 0.86 | 0.89 |
| *CG12333* | ts | **0.59** | *WDR37* | mr | 1.07 | **0.76** | 1.16 | 1.21 | 1.31 |

**Figure 3. miR-8 Targets USH in Fat Body to Regulate Body Growth**

(A) Upper: Sequence alignment of *Drosophila* miR-8 and human miR-200 family miRNAs. Lower: Genomic organization of the human miR-200 clusters.

(B) Schematic describing the bioinformatics procedure we used to identify common targets of miR-8 and miR-200.

(C) Summary of the results of the bioinformatics analyses and 3′ UTR reporter assays. Ts, Targetscan; pt, Pictar; mr, Miranda; mt, miTarget; and mc, microT. Eight gene pairs were validated by reporter assays in both *Drosophila* S2 (left) and human HeLa cells (right). The experiments were performed at least in duplicate, and the average fold change is presented. Levels of repression of 0.8-fold or more are shown in bold. Predicted targets that gave negative results in the 3′ UTR reporter assays are listed in Table S1.

(D) Upper: genetic rescue experiment by knockdown of miR-8 target genes. dsRNA was expressed in the fat body of miR-8 null larvae using the *CgGal4*, and the weights of adult male flies were measured ($n > 35$ for each genotype). Lower: USH knockdown in the fat body of wild-type larvae does not significantly alter the body weight ($n = 35$). $^{**}p < 2 \times 10^{-10}$ when compared with miR-8 null mutants with the GAL4 drivers alone.

(E) Introduction of heterozygous $ush^{1513}$ increases adult body weight ($n > 50$ male flies for each genotype). $^{\#}p < 4.1 \times 10^{-6}$, compared with miR-8 null flies.

(F) The ush mRNA is upregulated in the fat body of miR-8 null larvae. Measurements in triplicate.

(G) Upper: The USH protein level is increased in the fat body of miR-8 null larvae (lane 3). The negative control (lane 2) is the transheterozyote of a hypomorphic allele ($ush^{1513}$) and an amorphic allele ($ush^{vx22}$). Lower: Quantification of the level of USH in fat body of wild-type and miR-8 null larvae, from three independent batches. Error bars denote SEM.

Because a previous study showed that miR-8 targets *atrophin* (*atro*) to prevent neurodegeneration (Karres et al., 2007), we tested whether *atro* is also involved in body size regulation. Knockdown of *atro* in the fat body, however, failed to rescue the small body phenotype of miR-8 null flies (Figure 3D). Thus, the reported function of miR-8 in the prevention of neurodegeneration (Karres et al., 2007) may be separate from its function in body growth, not only spatially but also at the molecular level. To exclude possible off-target effects of *ush* RNAi, we used the $ush^{1513}$ hypomorph, which expresses a reduced level of *ush* as the result of a mutation in the promoter region (Cubadda et al., 1997). Consistent with the results of the *ush* RNAi, $ush^{1513}$ heterozygotes have larger adult bodies than do the control flies (Figure 3E). This result indicates that USH may indeed suppress body growth.

Next, we examined whether the level of USH was elevated in miR-8 null animals. The endogenous *ush* mRNA level was determined by qRT-PCR analysis of the RNAs from whole larva or larval fat body. The *ush* mRNA is, indeed, significantly upregulated in the fat body of miR-8 null larvae (~2.0 fold), suggesting

that miR-8 suppresses *ush* in the fat body (Figure 3F and Figure S3A). Upregulation of *ush* mRNA in whole larval RNA was less prominent (~1.3 fold) (Figure 3F). Thus, *ush* may be more strongly suppressed in the fat body than in other body parts. Notably, USH protein levels are more dramatically affected than the mRNA levels (Figure 3G and Figure S3B), indicating that miR-8 represses USH production by both mRNA destabilization and translational inhibition. Furthermore, a point mutation of the miR-8 target site in the 3′ UTR of *ush* abolished the suppression of the 3′ UTR reporter (Figure S4C), indicating that the suppression is mediated through the direct binding of miR-8 to the predicted target site. Putative target sites for miR-8 are found in all *Drosophila* species examined, including distant species such as *D. virilis* and *D. grimshawi* (data not shown). Together, these results demonstrate that *ush* is an authentic target of miR-8.

## miR-8 and USH Regulate PI3K

Several reports have suggested that insulin signaling in the larval fat body controls organismal growth in a non-cell-autonomous manner (Britton et al., 2002; Colombani et al., 2005). In support of this idea, we observed that suppression of insulin signaling in the larval fat body yielded smaller flies (Figure S5A) and fewer cells in the wing (Figure S5B). This phenotype is similar to that of miR-8 null flies (Figure 1D). To further investigate whether insulin signaling is indeed defective in the fat body of miR-8 null animals, we used the tGPH reporter, a GFP protein fused to a PH domain (Britton et al., 2002). Using this technique, the activity of PI3K can be measured by monitoring the membrane-associated GFP signal, because PH domains bind to the membrane-anchored phosphatidylinositol-3,4,5-triphosphate ($PIP_3$) produced by PI3K. We found that PI3K activity was downregulated in *mir-8* mutant fat bodies (Figure 4A, left panel) and that FOXO was more strongly localized to the nucleus of mutant fat bodies than the controls (Figure 4A, right panel). Moreover, the level of p-Akt was significantly reduced in the fat body (Figure S6A, left), whereas the phosphorylated JNK level did not change (Figure S6A, right). Thus, insulin signaling is specifically disrupted in the fat bodies of miR-8 null larvae.

To more precisely analyze miR-8's function in fat cells, flip-out GAL4 overexpressing clones of miR-8 were generated in the fat body of *mir-8* heterozygote. In the mosaic fat cells overexpressing miR-8, the tGPH signals was augmented in the membrane, indicating that miR-8 promotes PI3K activity in a cell-autonomous manner (Figure 4B). Cell size also increased with miR-8 overexpression (Figure 4B).

We next generated mitotic null clones to observe the loss of function phenotype. Cells of the miR-8 null clone were smaller than the adjacent cells in the twin spot—the cells harboring wild-type copies of miR-8 (Figure 4C and Figure S7). This suggests that miR-8 promotes fat cell growth in a cell-autonomous manner, as expected if miR-8 enhances insulin signaling in the fat body. We often found fewer (or no) null clone cells next to the twin spot cells when the mitotic clones were induced at embryonic stage or newly hatched larval stage. This suggests the frequent failure of proliferation and survival of miR-8 null cells during larval development (Figure 4C and data not shown). It is noted that we generated null clones of miR-8 in the wing or eye disc but found little growth defect in these organs (Figure S8). Therefore, the effect of miR-8 on cell growth is dependent on tissue type, which may be explained by the fact that USH is present in the fat body but not in wing precursor cells or the eye disc (Cubadda et al., 1997) (Figure S9).

To determine whether USH negatively regulates insulin signaling, mosaic clones of fat cells overexpressing USH were generated. USH-overexpressing cells were smaller in size and showed significantly lower tGPH signals in the membrane (Figure 4D and Figure S10) and higher FOXO signals in the nucleus than did the neighboring wild-type cells (Figure 4E). We also created mosaic fat cells expressing dsRNA against *ush* to observe the knockdown phenotype. The tGPH signal was significantly enhanced in the mosaic cells depleted of USH (Figure 4F). In mosaic *ush* mutant cells, the nuclear FOXO signals decreased (Figure 4G). Together, our observations indicate that USH inhibits insulin signaling upstream of or in parallel with PI3K in a cell-autonomous manner.

We further examined whether reduced insulin signaling caused by the absence of miR-8 could be rescued by knockdown of USH. Excessive insulin signaling is known to reduce the levels of insulin receptor (*Inr*) and cytohesin *Steppke* (*step*) through negative feedback by FOXO (Fuss et al., 2006; Puig and Tjian, 2005). These two targets of FOXO were upregulated in the fat body of miR-8 null larvae, whereas reintroduction of miR-8 dramatically reduced their expression (Figure 4H). Notably, ush RNAi also restores the mRNA levels of the FOXO target genes Inr and step in *mir-8* mutant fat bodies (Figure 4H). Thus, the defect of insulin signaling in the fat body of miR-8 null larvae is at least partially attributable to elevated *ush* levels.

## FOG2, a Target of miR-200, Regulates PI3K in Humans

The *ush* mRNA has one predicted binding site for miR-8, whereas the mammalian ortholog of *ush*, *FOG2*, has at least three predicted sites for miR-200 family miRNAs (Figures S4A and S4B). When all the putative sites in the 3′ UTR reporter of FOG2 are mutated (Figure 5A, m123), the reporter became refractory to the miR-200 family miRNAs. These predicted sites in the 3′ UTR of FOG2 are, therefore, responsible for miR-200-mediated FOG2 regulation. It is noted that miR-200a and miR-141 that have one nucleotide mismatch in the seed sequence suppressed the UTR reporter, albeit less effectively than the other members did (Figure S4D), suggesting that the noncanonical target sites may also lead to repression (Bartel, 2009; Brennecke et al., 2005).

FOG2 is expressed in the heart, brain, testes, liver, lung, and skeletal muscle (Holmes et al., 1999; Lu et al., 1999; Svensson et al., 1999; Tevosian et al., 1999). Despite its relatively broad expression in adult tissues, little is known about the function of FOG2 beyond its role in embryonic heart development (Fossett and Schulz, 2001). The miR-200 miRNAs have also been reported to be expressed in various adult organs, including pituitary gland, thyroid, pancreatic islet, testes, prostate, ovary, breast, and liver (Landgraf et al., 2007). We looked for a correlation between the expression of FOG2 protein and miR-200c cluster miRNAs in human cell lines derived from different organs (Figure S11). There is generally a negative correlation between miR-200 miRNAs and FOG2 in a given tissue type, consistent with a suppressive role for miR-200 in FOG2 regulation.

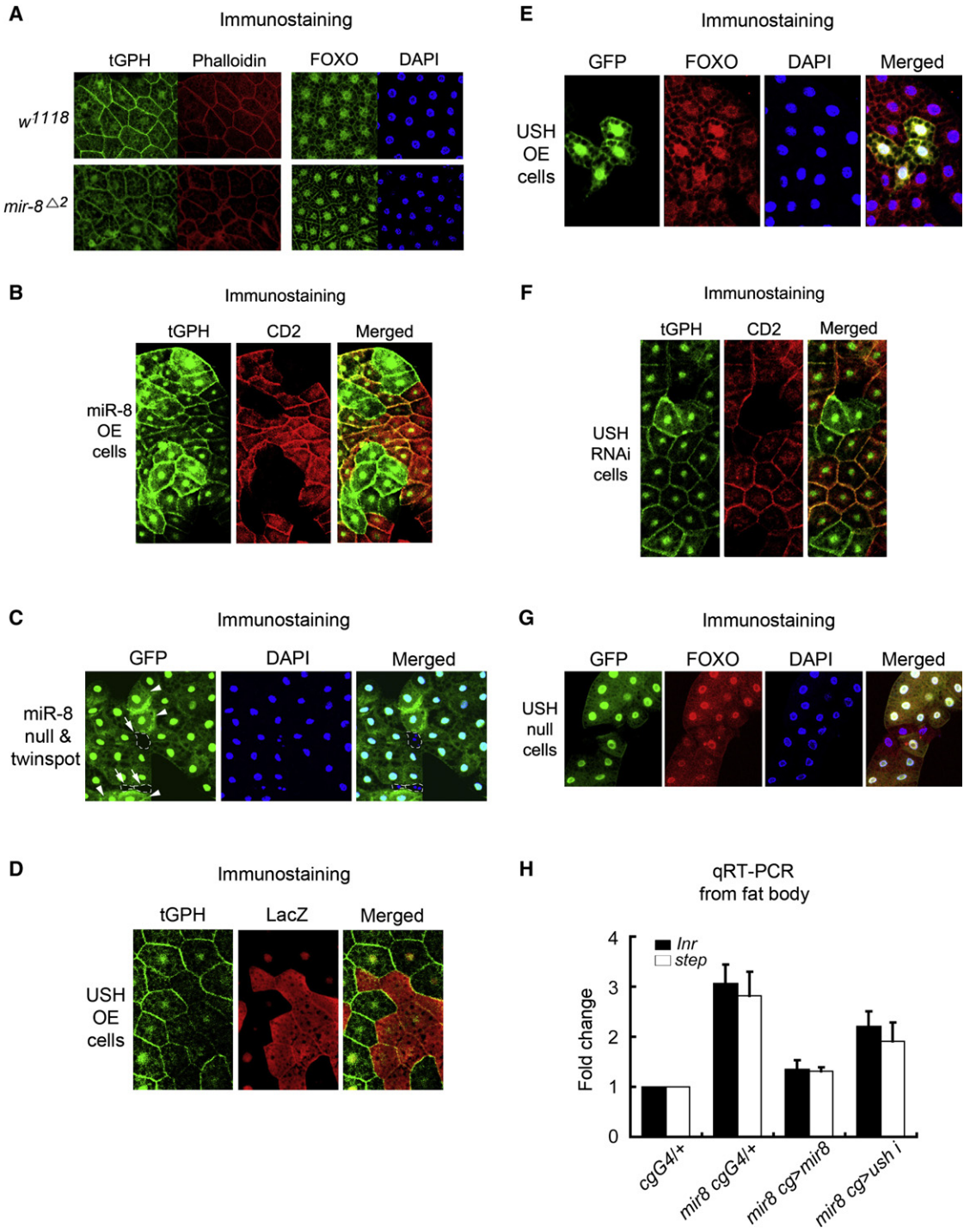


**Figure 4. miR-8 and USH Regulate PI3K-FOXO in Fat Body Cells**

(A) Left: Downregulation of PI3K activity is visualized by reduced GFP signal (tGPH) at the plasma membrane of miR-8 null fat body cells. Right: Enhanced nuclear localization of FOXO is visualized in miR-8 null fat body cells.

(B) Mosaic fat cells overexpressing miR-8 (marked by the absence of CD2) in *mir-8* heterozygote mutant show increased tGPH signals.

(C) Mitotic null clone and its twin spot of miR-8 null cells were generated to show that miR-8 null cells (arrow) grow more slowly and contain less DNA content than wild-type cells (arrowhead). Fragmentation of the nucleus is observed in some miR-8 null cells.

(D) Fat body cells overexpressing USH (marked by LacZ) show reduced tGPH signals at the plasma membrane. Leaky expression of LacZ not induced by GAL4 is shown in the nucleus of wild-type neighboring cells.

(E) Fat body cells overexpressing USH (marked by GFP) show enhanced nuclear localization of FOXO.

We next sought to confirm the repression of FOG2 by miR-200 miRNAs. Transfection of miR-200 miRNAs significantly reduced FOG2 protein levels (Figure 5B) in hepatocellular carcinoma Huh7 cells that express relatively low but detectable levels of miR-200 and FOG2 (Figure S11). In addition, the inhibition of miR-200 miRNAs by 2′-O-methyl oligonuclelotides antisense to miR-200 increased FOG2 protein levels in pancreatic cancer AsPC1 cells that express relatively high levels of miR-200 miRNAs (Figure 5C and Figure S11). These data demonstrate that FOG2 is an authentic target of endogenous miR-200 miRNAs.

Next, we investigated whether human miR-200 miRNAs have a conserved role in the modulation of insulin signaling, as in the case of fly miR-8 miRNA. Transfection of miR-200 increases p-Akt levels (Figure 5B), whereas miR-200 inhibitors reduce p-Akt levels (Figure 5C). Moreover, knockdown of FOG2 increased p-Akt levels, mimicking the effect of miR-200 (Figure 5D). We also tested the effect of FOG2 on PI3K activity by immunocomplex kinase assay using an antibody against p85α (Figure 5E). When Hep3B cells were transfected with a FOG2-expression plasmid, IGF-1 (Insulin like growth factor–1) failed to induce PI3K activity, indicating that FOG2 suppresses PI3K (Figure 5E). Consistent with this result, Akt was not phosphorylated in IGF-1–treated cells when FOG2 was ectopically introduced (Figure 5F). We further analyzed the effect of miR-200 miRNAs on the downstream transducers of Akt (Figure S12). Because activated Akt represses FOXO activity, we used a luciferase reporter plasmid (pFK1tk-luc) containing eight FOXO-binding sites (Biggs et al., 1999) to determine the level of FOXO activity in cultured cells. The activity of this FOXO reporter in Hep3B cells was significantly repressed by transfection of miR-200 miRNAs and by FOG2 knockdown (Figure S12A). Furthermore, treating the cells with miR-200 inhibitors elevated FOXO activity (Figure S12B). Consistently, when FOG2 was overexpressed, FOXO activity was upregulated (Figure S12C). In contrast to PI3K pathway components, the level of phosphorylated Erk was not significantly impaired (Figure S6B). In addition, inhibitors of JNK or Mek1/2 did not affect miR-200–mediated FOXO regulation, whereas PI3K inhibitor abrogated this FOXO regulation by miR-200 (Figure S6C). Thus, our data suggest that miR-200 specifically modulates PI3K-Akt-FOXO signaling.

Because stimulation of PI3K and Akt is known to facilitate cell proliferation and antagonize apoptosis (Pollak, 2008), we measured cellular viability with the MTT (3-(4,5-dimethylthiazol-2-yl)-2,5-diphenyltetrazolium bromide) assay in Hep3B cells. Introduction of miR-200 miRNAs increased cell viability (Figure S1B), whereas miRNA inhibitors produced the opposite effect (Figure S1C).

To investigate the action mechanism of FOG2, we performed Western blotting against p85α, p110, and IRS-1 following p85α immunoprecipitation (Figure 5G). Notably, when FOG2 was expressed, reduced amounts of p110 and IRS-1 were coprecipitated with p85α. Thus, FOG2 may act as a negative regulator of PI3K by interfering with the formation of a IRS-1/p85α/p110 complex.

### FOG2 Directly Binds to p85α to Inhibit PI3K

Although FOG2 is thought to be a nuclear transcriptional coregulator, several studies have reported that FOG2 also localizes to the cytoplasm (Bielinska et al., 2005; Clugston et al., 2008). To confirm this finding, we performed subcellular fractionation and Western blotting. FOG2 was, in fact, observed predominantly in the cytoplasm rather than in the nucleus in HeLa and PANC1 cells (Figure 6A). Immunostaining also showed cytoplasmic localization of FOG2 in HepG2 cells (Figure 6B), suggesting a cytoplasmic role of FOG2.

Given that FOG2 suppresses PI3K and colocalizes with p85α (Figures 5 and 6), we suspected that FOG2 may interact with PI3K. Notably, a significant amount of p85α, the regulatory subunit of PI3K, was coprecipitated with anti-FOG2 antibody (Figure 6C). Interaction between FOG2 and p85α was also observed when the FOG2 was ectopically expressed in a FLAG-tagged form (Figure 6D and Figure S13).

To map the interaction domain of FOG2, several truncated mutants of FOG2 were generated. The mutants containing a FLAG-tag in the N termini were coexpressed with V5-tagged p85α and were analyzed by immunoprecipitation using anti-FLAG antibody. The results indicate that the middle region of FOG2 (507–789 aa) mediates the interaction with p85α (Figure 6D). We then asked whether the middle region is sufficient to inhibit PI3K activity when it is ectopically expressed in HepG2 cells (Figure 6E). The middle region suppressed PI3K, whereas neither the N-terminal part nor the C-terminal part had a significant effect on PI3K activity (Figure 6E).

To test whether FOG2 binds to p85α directly, the FOG2 protein was expressed and purified from bacteria and was used in an in vitro binding assay, along with purified recombinant p85α protein fused to GST. The recombinant FOG2 protein containing the middle region of FOG2 (413-789 aa) specifically bound to recombinant p85α (Figure 6F).

Finally, we asked whether FOG2 can directly inhibit p85α by performing an in vitro PI3K assay using recombinant FOG2. Addition of the recombinant FOG2 protein containing the middle region (FOG2[413-789]) to the immunoprecipitated PI3K complex significantly inhibited the PI3K activity (Figure 6G). This finding suggests that direct binding of FOG2 to p85α leads to the inhibition of PI3K activity. Notably, we also found that *Drosophila* USH physically interacts with *Drosophila* p60 (dp60, the fly ortholog of p85α) when dp60 is coexpressed with USH in human HEK293T cells (Figure S14). Therefore, the action mechanism of USH/FOG2 may be conserved across the phyla.

## DISCUSSION

Our study reveals two novel regulatory components of insulin signaling: miR-8/miR-200 and USH/FOG2 (Figure 7). miR-8/200

(F) Mosaic fat cells depleted of USH (marked by the absence of CD2 signal) in *mir-8* heterozygous mutant show an increase of tGPH signal.
(G) Fat cells homozygous for $ush^{vx22}$ (marked by the absence of GFP signal), a putative amorphic mutant of *ush*, show reduced nuclear localization of FOXO.
(H) Expression of miR-8 or dsRNA of *ush* in the fat body reactivates insulin signaling, as measured by qRT-PCR of *Inr* and *step* in the larval fat body. Error bars denote the SEM.

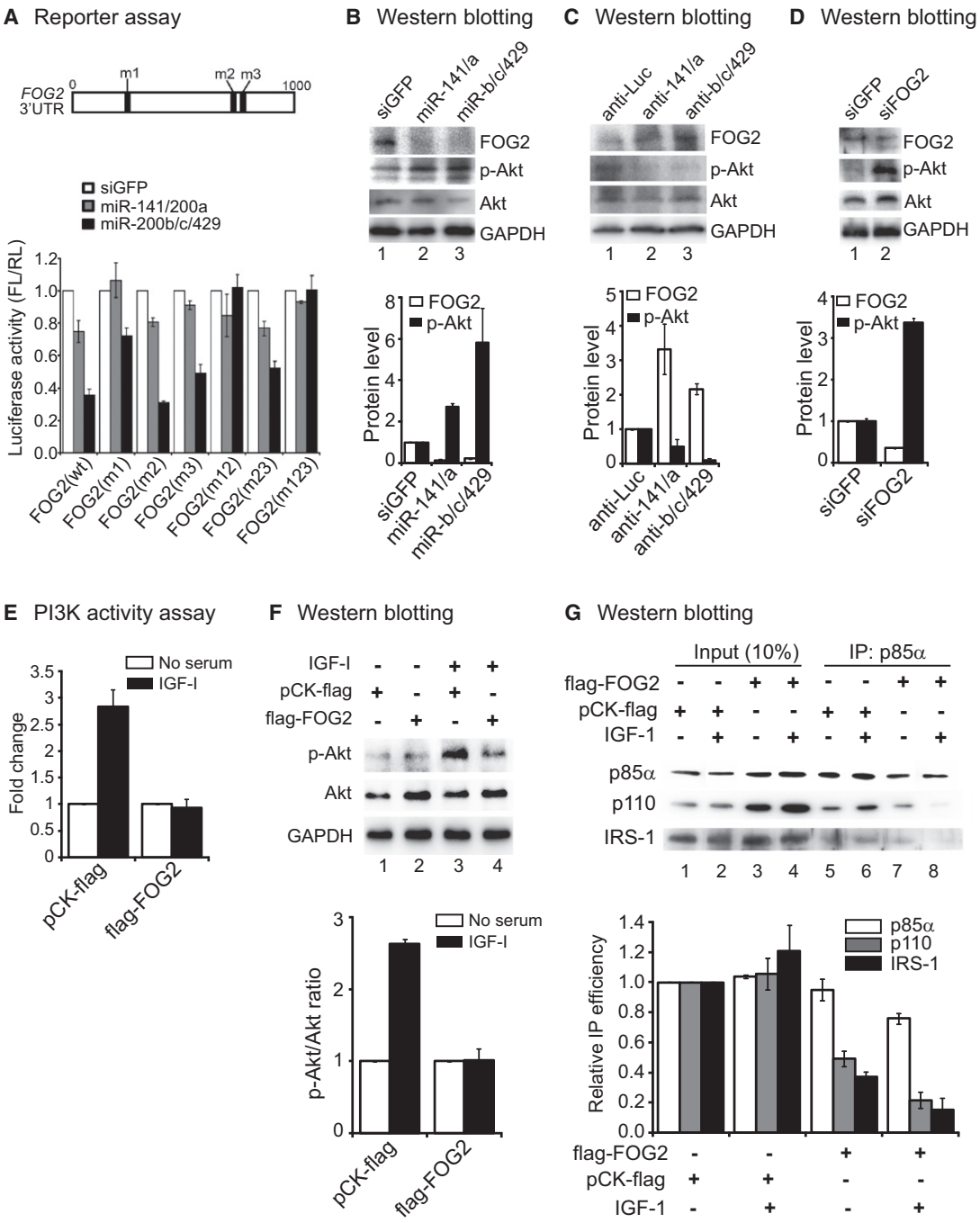


**Figure 5. FOG2 Is Targeted by miR-200 to Regulate PI3K-Akt**

(A) Site-directed mutagenesis of three target sites in the 3′ UTR of FOG2. miRNAs with identical seed sequences were pooled in equal amounts, and the mixture (30 nM in total) was transfected into HeLa cells; miR-141/200a and miR-200b/c/429 ($n$ = 3, mean ± SEM).

(B) miR-200 miRNAs downregulate the FOG2 protein level, resulting in an increase of p-Akt in Huh7 cells. siRNA against GFP (siGFP) was used as a negative control ($n$ = 3, mean ± SEM).

(C) Inhibitors against miR-200 miRNAs upregulate FOG2 and downregulate p-Akt in AsPC1 cells ($n$ = 3, mean ± SEM).

(D) siRNA against FOG2 (*siFog2*) increases the p-Akt level in FAO cells ($n$ = 3, mean ± SEM).

(E) Ectopic expression of FOG2 suppresses IGF-1-induced PI3K activity. Hep3B cells were treated with IGF-1 (100 ng/ml) for 20 min ($n$ = 3, mean ± SEM).

(F) Ectopic expression of FOG2 suppresses IGF-1-induced p-Akt. Hep3B cells were treated with IGF-1 (100 ng/ml) for 20 min ($n$ = 3, mean ± SEM).

(G) Ectopic expression of FOG2 disturbs the formation of an active PI3K complex containing p85α, p110, and IRS-1. Quantification from three biological replicates is shown in lower panel. Error bars denote the SEM.

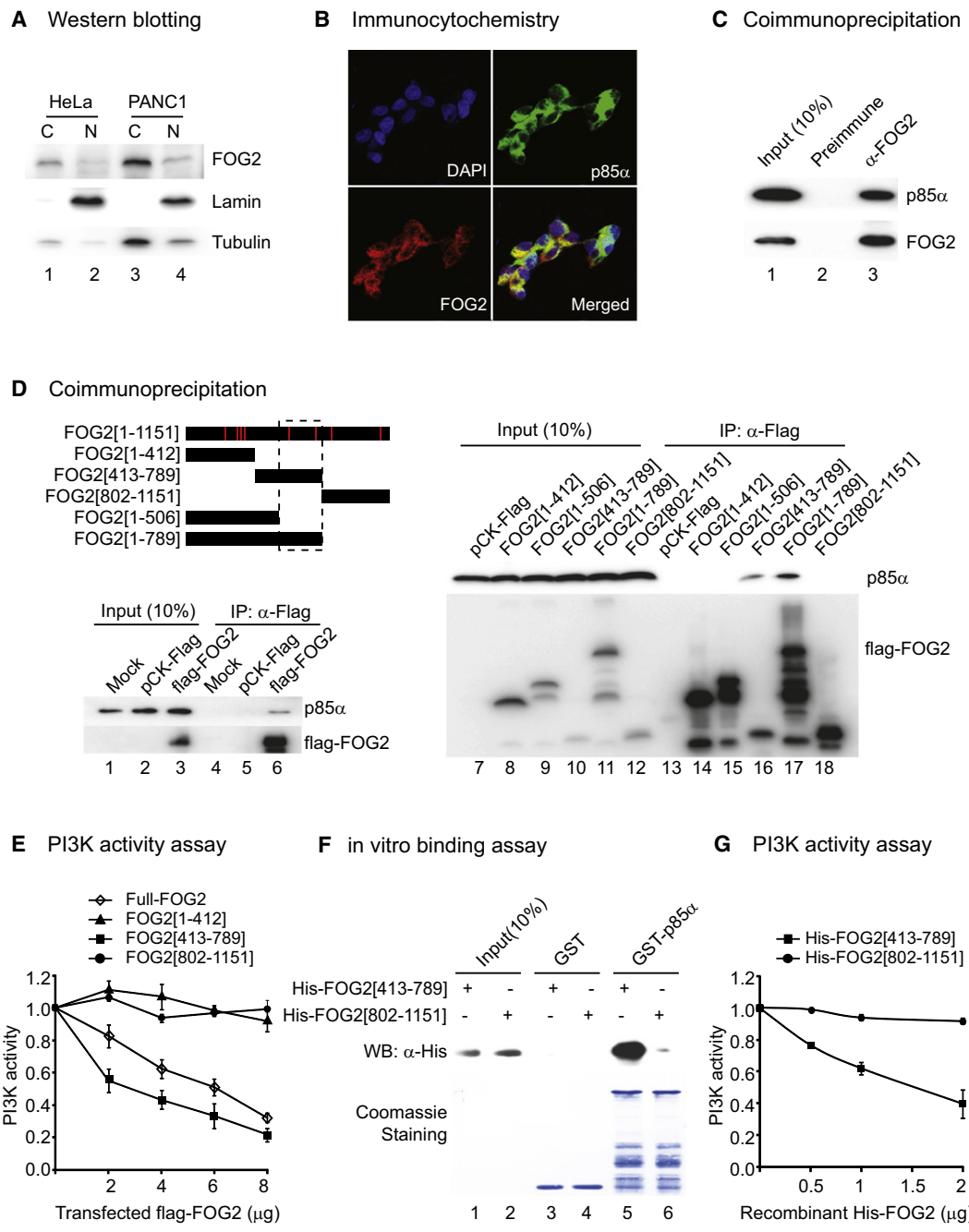


**Figure 6. FOG2 Directly Binds to p85α to Inhibit PI3K**

(A) Cytoplasmic localization of FOG2. The nuclear ("N") and cytosolic ("C") fractions of HeLa and PANC1 cells were analyzed by Western blotting with anti-FOG2 antibody. Lamin and tubulin were used as nuclear and cytoplasmic markers, respectively.

(B) Endogenous FOG2 is visualized in HepG2 cell by using anti-FOG2 antibody.

(C) Coimmunoprecipitation of p85α with FOG2. Endogenous FOG2 was immunoprecipitated with anti-FOG2 antibody from total cell extract from PANC1 cells. Zinc chloride was added, instead of EDTA, to IP buffer, which we found increased the affinity between p85α and FOG2. Western blot analysis was performed with anti-p85α and anti-FOG2 antibodies.

(D) Upper left: Schematic representation of full-length (1–1151) and five truncated FOG2 proteins. Red boxes indicate the location of zinc finger motifs. Lower left and right: Coimmunoprecipitation of p85α with Flag-tagged FOG2 in HepG2 cells. Note that the IP efficiency is lower in this experiment because the IP buffer contains EDTA, not zinc chloride.

(E) The truncated FOG2 containing the middle region (413–789 aa) inhibits PI3K activity in vivo ($n$ = 3, mean ± SEM).

(F) In vitro binding assay shows direct interaction between recombinant GST-p85α and recombinant His-FOG2[413-789].

(G) Dose-dependent reduction of PI3K activity by recombinant His-FOG2[413–789] ($n$ = 3, mean ± SEM).

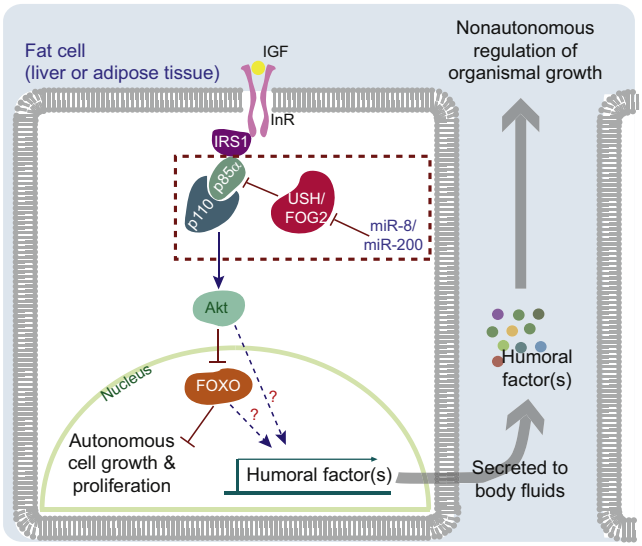


**Figure 7. Model for the Functions of miR-8/miR-200 and USH/FOG2**

In *Drosophila*, miR-8 posttranscriptionally represses USH, thereby activating insulin signaling, which results in cell-autonomous growth of fat body cells. This process also causes nonautonomous organismal growth, likely through the induction of humoral factors. In human liver cells, miR-200 posttranscriptionally represses FOG2, which directly binds to p85α and blocks the formation of an active PI3K complex. As such, the repression of FOG2 by miR-200 stimulates insulin signaling and cell proliferation.

negatively regulates USH/FOG2 through direct base-pairing to the 3′ UTR of the *ush/FOG2* mRNA. USH/FOG2, in turn, inhibits the formation of an active PI3K complex via direct interaction with dp60/p85α, the regulatory subunit of PI3K. In fly fat bodies, miR-8 suppresses *ush*, which causes cell-autonomous increase of fat cell growth (see Figure 7 for a model). The roles of miR-8 and USH are conserved in mammals; miR-200 miRNAs target FOG2 to upregulate insulin signaling and cell proliferation in human cells. Given that the PI3K-Akt-FOXO pathway plays central roles in many developmental processes and that defects of this pathway have been associated with cancer, diabetes, neuropathology, and aging (Arden, 2008; Pollak, 2008), further investigation of the miR-8/200 family and USH/FOG2 may contribute to the understanding and amelioration of such human diseases.

Our results support and extend the emerging theory that the fat body is a central organ coordinating metabolic condition and global growth of the organism. We propose that miR-8 regulates the growth of peripheral tissues in a non-cell-autonomous manner by modulating the secretion of the humoral factors that are under the control of insulin signaling (Figure 7). Future investigation is needed to identify the humoral factors that mediate the communication between the fat body and other tissues. Because the larval fat body is considered the *Drosophila* counterpart of mammalian liver and adipose tissues (Leopold and Perrimon, 2007), it will be interesting to study whether miR-200 and FOG2 play a similar role in liver and adipose tissues to control body growth during the human juvenile period.

Previous studies suggest that USH/FOG2 may function as either transcriptional coactivators or corepressors by partnering with various GATA transcription factors. However, FOG2 is localized to the cytoplasm in some tissues (Bielinska et al., 2005; Clugston et al., 2008) (Figure 6A). FOG1, the other human homolog of *Drosophila* USH, was also reported to remain in the cytoplasm of skin stem cells that lack GATA-3 (Kaufman et al., 2003) and was shown to be sequestered in the cytoplasm by a cytoplasmic protein TACC3 (Garriga-Canut and Orkin, 2004). USH/FOG2 have been studied mainly in hematopoiesis and heart development in both flies and mammals (Fossett and Schulz, 2001; Fossett et al., 2001; Holmes et al., 1999; Lu et al., 1999; Svensson et al., 1999; Tevosian et al., 1999). However, it was recently shown that USH suppresses cell proliferation in *Drosophila* hemocytes (Sorrentino et al., 2007). It is also noteworthy that FOG2 is frequently downregulated in human cancers of the thyroid (NCBI GEO accession: GSE3678), lung (Wachi et al., 2005), and prostate (Nanni et al., 2006), which suggests a role of FOG2 as a tumor suppressor. To our knowledge, our study reports for the first time that FOG2 acts as a negative modulator of the PI3K-Akt pathway via direct binding to p85α. It remains to be determined whether the newly discovered molecular function of USH/FOG2 is related to the previously described phenotypes of *ush/FOG2*.

Our study also offers a comprehensive way of discovering the physiological function of conserved miRNAs. By systematically mapping the protein homologs of miRNA targets and by validating them experimentally, we identified seven gene pairs as conserved targets of the miR-8/200 family. We also used fly genetics and human cell biology to identify *ush/FOG2* as the target gene that is responsible for one particular phenotype. Of note, six other genes (*Lap1/ERBB2IP*, *CG8445/BAP1*, *dbo/KLHL20*, *Lar/PTPRD*, *Ced-12/ELMO2*, and *CG12333/WDR37*) may also be authentic targets of miR-8/200, although they need to be further verified by additional methods. These six genes may function in different organs and/or at different developmental stages. Cohen and colleagues previously reported that miR-8 prevents neurodegeneration by targeting *atro* (Karres et al., 2007). We observe that *atro* knockdown does not rescue the small body phenotype of *mir-8* mutants (Figure 3D) and that *ush* knockdown cannot reverse the wing and leg defects attributed to *atro* (data not shown). Thus, a single miRNA may have several distinct functions in different cell types, likely depending on the availability of specific targets or downstream effectors. In a recent study, miR-8 gain of function was shown to affect the WNT pathway, although this finding was not sufficiently supported by the phenotype resulting from miR-8 loss of function (Kennell et al., 2008). The miR-200 family has also been shown to interfere with epithelial to mesenchymal transitions in humans (Gregory et al., 2008) to enhance cancer cell colonization in distant tissues (Dykxhoorn et al., 2009) and to regulate olfactory neurogenesis and osmotic stress in zebrafish (Choi et al., 2008; Flynt et al., 2009). It remains to be determined whether these previously described functions of the miR-8/200 microRNAs are systemically interconnected in a single organism and how widely each of these functions is conserved among animals expressing miR-8/200 microRNAs.

## EXPERIMENTAL PROCEDURES

### Fly Strains

*mir-8*$^{\Delta 2}$ mutant was a generous gift from Steve Cohen, and *mir-8 gal4* (P{GawB}NP5427) was obtained from the Kyoto Stock Centre. *FRT42D mir-8*$^{\Delta 2}$ fly was generated following conventional recombination procedure and was selected for G418 resistance of FRT. *UAS-ush*, *ush*$^{1513}$, and *ush*$^{vx22}$ were generous gifts of Pascal Heitzler, Pat Simpson, and K. VijayRaghavan. *FRT40A ush*$^{vx22}$ was a generous gift from Marc Haenlin. *Cg gal4* and *ppl gal4* were kindly provided by YoungJoon Kim and M. Pankratz, respectively. UAS-RNAi lines used in this study were purchased from the Vienna RNAi Library Centre. *ush gal4* (P{GawB}ush$^{MD751}$), *UAS-PI3KDN* (P{Dp110D954A}), *Aygal4 UAS-GFP, Aygal4 UAS-LacZ*, *tGPH*, and *FRT42D EGUF/hid* fly (BL-5251) stocks were obtained from the Bloomington *Drosophila* Stock Center. *Act > CD2 > gal4; tGPH* was a generous gift from Bruce Edgar.

### Measurement of Weight, Size, Pupariation, and Adult Emergence

Flies were grown on standard fly food at 25°C. Groups of five animals were weighed 3–5 days after eclosion. All flies were ice-anesthetized before weight measurement. To examine the time of pupariation and adult emergence, eggs were collected for 5 hr, and the number of new pupa or adults were counted every 12 hr.

### Clonal Analysis

Mitotic null clones in larval fat body were generated by heat shock at 39°C for 2 hr right after collection of eggs for 9 hr. For inducing the flip-out GAL4 overexpression clone, embryos and newly hatched larva were heat shocked at 39°C for 10 min.

### Immunostaining

Mid-third instar larvae (96 hr AEL) were dissected and fixed in 4% formaldehyde and blocked as previously described (Lee et al., 2005), except in the case of tGPH visualization. For tGPH staining, Zamboni's fixative (4% paraformaldehyde and 7.5% saturated picric acid in PBS) was used for tissue fixation. Antibodies against GFP (1:200, Sigma), LacZ (1:1000, Promega), CD2 (1:200, Serotec), and FOXO (1:500, a gift from O. Puig) were used. Anti-mouse Alexa 488/594 and anti-rabbit Alexa 488/594 secondary antibodies (1:200, Molecular Probes) were used. To visualize cell membranes, phalloidin-TRITC (Sigma) was added during secondary antibody incubation. DAPI was used for DNA staining. The images were obtained with a Zeiss LSM510 confocal microscope.

### Immunoprecipitation and PI3K Assay

Hep3B cell lysates were prepared using lysis buffer (137 mM NaCl, 20 mM Tris-HCl [pH 7.4], 1 mM $CaCl_2$, 1 mM $MgCl_2$, 0.1 mM sodium orthovanadate, and 1% NP-40), and PI3K was immunoprecipitated with anti-p85$\alpha$ monoclonal antibody (sc-1637, Santa Cruz). Immunocomplexes were collected on protein A-Sepharose beads, washed twice with lysis buffer, and washed twice with wash buffer (0.1 M Tris-HCl [pH 7.4], 5 mM LiCl, and 0.1 mM sodium orthovanadate). PI3K activity was assayed by adding 10 $\mu$g of sonicated PIP2 (Calbiochem) and 1 $\mu$l of [$\gamma$-$^{32}$P]ATP (500 $\mu$Ci/ml) in 60 $\mu$l of kinase assay buffer (10 mM Tris-HCl [pH 7.4], 150 mM NaCl, 1 mM sodium orthovanadate, and 10 $\mu$l of 100 mM $MgCl_2$). The reactions were terminated after 20 min at 37°C by the addition of 20 $\mu$l of 6N HCl. The lipids were extracted with $CHCl_3$:MeOH (1:1) and were analyzed using scintillation counter. For in vitro PI3K activity assay, the immunocomplexes were incubated with purified His-tagged FOG2 proteins for 2 hr at 4°C.

## SUPPLEMENTAL DATA

Supplemental data include Supplemental Experimental Procedures, 3 tables, and 14 figures and can be found with this article online at http://www.cell.com/supplemental/S0092-8674(09)01432-9.

## ACKNOWLEDGMENTS

We are very grateful to Drs. Steve Cohen, Pascal Heitzler, Pat Simpson, K. VijayRaghavan, Bruce Edgar, YoungJoon Kim and Marc Haenlin for kindly sharing fly lines. We appreciate the help of Drs. Kweon Yu and Kyu-Sun Lee for immunostaining. We thank Dr. Elisa Izaurralde for the pAC5.1 luciferase vector and Dr. Seunghwan Hong for GST-p85$\alpha$. We are also grateful to Dr. Jeongbin Yim and his lab members for providing the equipment for fly work, Jisun Yoo for help with reporter cloning, and Dr. Walton Jones, Dr. Chirlmin Joo, Jinju Han, and David Jee for critical reading of the manuscript. This work was supported by the Creative Research Initiatives Programs (grant 20090063603 to V.N.K. and grant R16-2001-002-01001-0 to J.C.), the National Research Foundation of Korea, BK21 Research Fellowships from the Ministry of Education, Science and Technology of Korea (support to H.J.), and the Seoul Science Fellowship (support to H.J.).

Received: June 4, 2009
Revised: September 21, 2009
Accepted: November 10, 2009
Published: December 10, 2009

## REFERENCES

Arden, K.C. (2008). FOXO animal models reveal a variety of diverse roles for FOXO transcription factors. Oncogene *27*, 2345–2350.

Asha, H., Nagy, I., Kovacs, G., Stetson, D., Ando, I., and Dearolf, C.R. (2003). Analysis of Ras-induced overproliferation in *Drosophila* hemocytes. Genetics *163*, 203–215.

Baker, J., Liu, J.P., Robertson, E.J., and Efstratiadis, A. (1993). Role of insulin-like growth factors in embryonic and postnatal growth. Cell *75*, 73–82.

Bartel, D.P. (2009). MicroRNAs: target recognition and regulatory functions. Cell *136*, 215–233.

Bielinska, M., Genova, E., Boime, I., Parviainen, H., Kiiveri, S., Leppaluoto, J., Rahman, N., Heikinheimo, M., and Wilson, D.B. (2005). Gonadotropin-induced adrenocortical neoplasia in NU/J nude mice. Endocrinology *146*, 3975–3984.

Biggs, W.H., 3rd, Meisenhelder, J., Hunter, T., Cavenee, W.K., and Arden, K.C. (1999). Protein kinase B/Akt-mediated phosphorylation promotes nuclear exclusion of the winged helix transcription factor FKHR1. Proc. Natl. Acad. Sci. USA *96*, 7421–7426.

Brennecke, J., Stark, A., Russell, R.B., and Cohen, S.M. (2005). Principles of microRNA-target recognition. PLoS Biol. *3*, e85.

Britton, J.S., Lockwood, W.K., Li, L., Cohen, S.M., and Edgar, B.A. (2002). *Drosophila's* insulin/PI3-kinase pathway coordinates cellular metabolism with nutritional conditions. Dev. Cell *2*, 239–249.

Caldwell, P.E., Walkiewicz, M., and Stern, M. (2005). Ras activity in the *Drosophila* prothoracic gland regulates body size and developmental rate via ecdysone release. Curr. Biol. *15*, 1785–1795.

Choi, P.S., Zakhary, L., Choi, W.Y., Caron, S., Alvarez-Saavedra, E., Miska, E.A., McManus, M., Harfe, B., Giraldez, A.J., Horvitz, R.H., et al. (2008). Members of the miRNA-200 family regulate olfactory neurogenesis. Neuron *57*, 41–55.

Clugston, R.D., Zhang, W., and Greer, J.J. (2008). Gene expression in the developing diaphragm: significance for congenital diaphragmatic hernia. Am. J. Physiol. Lung Cell. Mol. Physiol. *294*, L665–L675.

Colombani, J., Bianchini, L., Layalle, S., Pondeville, E., Dauphin-Villemant, C., Antoniewski, C., Carre, C., Noselli, S., and Leopold, P. (2005). Antagonistic actions of ecdysone and insulins determine final size in *Drosophila*. Science *310*, 667–670.

Colombani, J., Raisin, S., Pantalacci, S., Radimerski, T., Montagne, J., and Leopold, P. (2003). A nutrient sensor mechanism controls *Drosophila* growth. Cell *114*, 739–749.

Cubadda, Y., Heitzler, P., Ray, R.P., Bourouis, M., Ramain, P., Gelbart, W., Simpson, P., and Haenlin, M. (1997). u-shaped encodes a zinc finger protein

that regulates the proneural genes achaete and scute during the formation of bristles in *Drosophila*. Genes Dev. *11*, 3083–3095.

Dykxhoorn, D.M., Wu, Y., Xie, H., Yu, F., Lal, A., Petrocca, F., Martinvalet, D., Song, E., Lim, B., and Lieberman, J. (2009). miR-200 enhances mouse breast cancer cell colonization to form distant metastases. PLoS One *4*, e7181.

Edgar, B.A. (2006). How flies get their size: genetics meets physiology. Nat. Rev. Genet. *7*, 907–916.

Flynt, A.S., Thatcher, E.J., Burkewitz, K., Li, N., Liu, Y., and Patton, J.G. (2009). miR-8 microRNAs regulate the response to osmotic stress in zebrafish embryos. J. Cell Biol. *185*, 115–127.

Fossett, N., and Schulz, R.A. (2001). Conserved cardiogenic functions of the multitype zinc-finger proteins: U-shaped and FOG-2. Trends Cardiovasc. Med. *11*, 185–190.

Fossett, N., Tevosian, S.G., Gajewski, K., Zhang, Q., Orkin, S.H., and Schulz, R.A. (2001). The Friend of GATA proteins U-shaped, FOG-1, and FOG-2 function as negative regulators of blood, heart, and eye development in *Drosophila*. Proc. Natl. Acad. Sci. USA *98*, 7342–7347.

Fuss, B., Becker, T., Zinke, I., and Hoch, M. (2006). The cytohesin Steppke is essential for insulin signalling in *Drosophila*. Nature *444*, 945–948.

Garriga-Canut, M., and Orkin, S.H. (2004). Transforming acidic coiled-coil protein 3 (TACC3) controls friend of GATA-1 (FOG-1) subcellular localization and regulates the association between GATA-1 and FOG-1 during hematopoiesis. J. Biol. Chem. *279*, 23597–23605.

Gregory, P.A., Bracken, C.P., Bert, A.G., and Goodall, G.J. (2008). MicroRNAs as regulators of epithelial-mesenchymal transition. Cell Cycle *7*, 3112–3118.

Holmes, M., Turner, J., Fox, A., Chisholm, O., Crossley, M., and Chong, B. (1999). hFOG-2, a novel zinc finger protein, binds the co-repressor mCtBP2 and modulates GATA-mediated activation. J. Biol. Chem. *274*, 23491–23498.

Ikeya, T., Galic, M., Belawat, P., Nairz, K., and Hafen, E. (2002). Nutrient-dependent expression of insulin-like peptides from neuroendocrine cells in the CNS contributes to growth regulation in *Drosophila*. Curr. Biol. *12*, 1293–1300.

Iorio, M.V., Visone, R., Di Leva, G., Donati, V., Petrocca, F., Casalini, P., Taccioli, C., Volinia, S., Liu, C.G., Alder, H., et al. (2007). MicroRNA signatures in human ovarian cancer. Cancer Res. *67*, 8699–8707.

John, B., Enright, A.J., Aravin, A., Tuschl, T., Sander, C., and Marks, D.S. (2004). Human MicroRNA targets. PLoS Biol. *2*, e363.

Karres, J.S., Hilgers, V., Carrera, I., Treisman, J., and Cohen, S.M. (2007). The conserved microRNA miR-8 tunes atrophin levels to prevent neurodegeneration in *Drosophila*. Cell *131*, 136–145.

Kaufman, C.K., Zhou, P., Pasolli, H.A., Rendl, M., Bolotin, D., Lim, K.C., Dai, X., Alegre, M.L., and Fuchs, E. (2003). GATA-3: an unexpected regulator of cell lineage determination in skin. Genes Dev. *17*, 2108–2122.

Kennell, J.A., Gerin, I., MacDougald, O.A., and Cadigan, K.M. (2008). The microRNA miR-8 is a conserved negative regulator of Wnt signaling. Proc. Natl. Acad. Sci. USA *105*, 15417–15422.

Kim, S.K., Nam, J.W., Rhee, J.K., Lee, W.J., and Zhang, B.T. (2006). miTarget: microRNA target gene prediction using a support vector machine. BMC Bioinformatics *7*, 411.

Kiriakidou, M., Nelson, P.T., Kouranov, A., Fitziev, P., Bouyioukos, C., Mourelatos, Z., and Hatzigeorgiou, A. (2004). A combined computational-experimental approach predicts human microRNA targets. Genes Dev. *18*, 1165–1178.

Krek, A., Grun, D., Poy, M.N., Wolf, R., Rosenberg, L., Epstein, E.J., MacMenamin, P., da Piedade, I., Gunsalus, K.C., Stoffel, M., et al. (2005). Combinatorial microRNA target predictions. Nat. Genet. *37*, 495–500.

Landgraf, P., Rusu, M., Sheridan, R., Sewer, A., Iovino, N., Aravin, A., Pfeffer, S., Rice, A., Kamphorst, A.O., Landthaler, M., et al. (2007). A mammalian microRNA expression atlas based on small RNA library sequencing. Cell *129*, 1401–1414.

Layalle, S., Arquier, N., and Leopold, P. (2008). The TOR pathway couples nutrition and developmental timing in *Drosophila*. Dev. Cell *15*, 568–577.

Lee, Y., Lee, J., Bang, S., Hyun, S., Kang, J., Hong, S.T., Bae, E., Kaang, B.K., and Kim, J. (2005). Pyrexia is a new thermal transient receptor potential channel endowing tolerance to high temperatures in *Drosophila melanogaster*. Nat. Genet. *37*, 305–310.

Leopold, P., and Perrimon, N. (2007). *Drosophila* and the genetics of the internal milieu. Nature *450*, 186–188.

Lewis, B.P., Burge, C.B., and Bartel, D.P. (2005). Conserved seed pairing, often flanked by adenosines, indicates that thousands of human genes are microRNA targets. Cell *120*, 15–20.

Lu, J.R., McKinsey, T.A., Xu, H., Wang, D.Z., Richardson, J.A., and Olson, E.N. (1999). FOG-2, a heart- and brain-enriched cofactor for GATA transcription factors. Mol. Cell. Biol. *19*, 4495–4502.

Mirth, C., Truman, J.W., and Riddiford, L.M. (2005). The role of the prothoracic gland in determining critical weight for metamorphosis in *Drosophila melanogaster*. Curr. Biol. *15*, 1796–1807.

Mirth, C.K., and Riddiford, L.M. (2007). Size assessment and growth control: how adult size is determined in insects. Bioessays *29*, 344–355.

Nam, E.J., Yoon, H., Kim, S.W., Kim, H., Kim, Y.T., Kim, J.H., Kim, J.W., and Kim, S. (2008). MicroRNA expression profiles in serous ovarian carcinoma. Clin. Cancer Res. *14*, 2690–2695.

Nanni, S., Priolo, C., Grasselli, A., D'Eletto, M., Merola, R., Moretti, F., Gallucci, M., De Carli, P., Sentinelli, S., Cianciulli, A.M., et al. (2006). Epithelial-restricted gene profile of primary cultures from human prostate tumors: a molecular approach to predict clinical behavior of prostate cancer. Mol. Cancer Res. *4*, 79–92.

Park, S.Y., Lee, J.H., Ha, M., Nam, J.W., and Kim, V.N. (2009). miR-29 miRNAs activate p53 by targeting p85 alpha and CDC42. Nat. Struct. Mol. Biol. *16*, 23–29.

Pollak, M. (2008). Insulin and insulin-like growth factor signalling in neoplasia. Nat. Rev. Cancer *8*, 915–928.

Puig, O., and Tjian, R. (2005). Transcriptional feedback control of insulin receptor by dFOXO/FOXO1. Genes Dev. *19*, 2435–2446.

Rulifson, E.J., Kim, S.K., and Nusse, R. (2002). Ablation of insulin-producing neurons in flies: growth and diabetic phenotypes. Science *296*, 1118–1120.

Smibert, P., and Lai, E.C. (2008). Lessons from microRNA mutants in worms, flies and mice. Cell Cycle *7*, 2500–2508.

Sorrentino, R.P., Tokusumi, T., and Schulz, R.A. (2007). The Friend of GATA protein U-shaped functions as a hematopoietic tumor suppressor in *Drosophila*. Dev. Biol. *311*, 311–323.

Stark, A., Brennecke, J., Russell, R.B., and Cohen, S.M. (2003). Identification of *Drosophila* MicroRNA targets. PLoS Biol. *1*, E60.

Svensson, E.C., Tufts, R.L., Polk, C.E., and Leiden, J.M. (1999). Molecular cloning of FOG-2: a modulator of transcription factor GATA-4 in cardiomyocytes. Proc. Natl. Acad. Sci. USA *96*, 956–961.

Takata, K., Yoshida, H., Yamaguchi, M., and Sakaguchi, K. (2004). *Drosophila* damaged DNA-binding protein 1 is an essential factor for development. Genetics *168*, 855–865.

Tevosian, S.G., Deconinck, A.E., Cantor, A.B., Rieff, H.I., Fujiwara, Y., Corfas, G., and Orkin, S.H. (1999). FOG-2: A novel GATA-family cofactor related to multitype zinc-finger proteins Friend of GATA-1 and U-shaped. Proc. Natl. Acad. Sci. USA *96*, 950–955.

Wachi, S., Yoneda, K., and Wu, R. (2005). Interactome-transcriptome analysis reveals the high centrality of genes differentially expressed in lung cancer tissues. Bioinformatics *21*, 4205–4208.

Zinke, I., Kirchner, C., Chao, L.C., Tetzlaff, M.T., and Pankratz, M.J. (1999). Suppression of food intake and growth by amino acids in *Drosophila*: the role of pumpless, a fat body expressed gene with homology to vertebrate glycine cleavage system. Development *126*, 5275–5284.